NMR Structure of an Antisense DNA·RNA Hybrid Duplex Containing a 3′-$CH_2N(CH_3)$-O-5′ or an MMI Backbone Linker†

Xueyong Yang,‡ Xiaogang Han,‡ Collin Cross,‡ Simona Bare,‡ Yogesh Sanghvi,§ and Xiaolian Gao*,‡

Department of Chemistry, University of Houston, 4800 Calhoun Street, Houston, Texas 77204-5641, and ISIS Pharmaceuticals, Inc., 2280 Faraday Avenue, Carlsbad, California 92008

Received February 26, 1999; Revised Manuscript Received June 28, 1999

ABSTRACT: The solution structure of an antisense DNA·RNA hybrid duplex, d(CGCGTT-MMI-TTGCGC)·r(GCGCAAAACGCG) (designated R4), containing an MMI backbone linker [3′-$CH_2N(CH_3)$-O5′], is elucidated. The structural details of the MMI linker, its structural effects on the neighboring residues, and the molecular basis of the MMI effects are examined. The lipophilic *N*-methyl group of MMI is peripheral to the helix, assuming a conformation that is most stable with regard to the N−O torsion angle. The MMI linker promotes a 3′-endo conformation for the sugar moieties at both 3′- and 5′-adjacent positions and a backbone kink involving distant residues along the 3′-direction. Comparison of R4 with other analogous hybrid duplexes previously studied in this laboratory reveals a new family of low-energy helical conformations that can be accommodated in stable duplexes and a common feature of C3′-modified sugars for adopting a C3′-endo pucker. The results of these studies emphasize the interplay of several factors that govern the formation of stable hybrid duplexes and provide a basis for the understanding of the biological role of the MMI modifications, which are important building blocks for a family of promising chimeric antisense oligonucleotides.

Backbone-modified oligonucleotide analogues have great potential to become effective therapeutics for various human diseases, due to their promises of improved cell permeability, enhanced resistance to enzymatic degradation, and tailored RNA binding properties (*1*−*3*). Upon the analogues binding to target RNA, the hybrid duplexes that are formed are substrates of RNA nucleases, such as RNase H, resulting in RNA inactivation. Unfortunately, although a large number of backbone modifications have been incorporated into oligonucleotides (*4*, *5*), there are only a limited few that actually meet the stringent requirements for antisense applications. In fact, even for these better chemical modifications, such as phosphorthioates [PS, 3′-O-PO(S)-O-5′] (*6*), there are problems that remain to be addressed. For instance, it is preferable to maintain a low level of use of sulfur in oligonucleotides to minimize cytotoxicity, which is likely due to the nonspecific binding of the sulfur-containing molecules to biofluid species. Therefore, continued demands exist for creating oligonucleotide analogues possessing combined desirable antisense properties, such as efficient cell permeability, cellular stability, and target specificity. To meet such demands, an understanding of not only the chemistry of modifications but also their patterns of incorporation should be achieved.

The MMI[1] (methylene methylimino, Scheme 1) backbone-modified oligonucleotides have recently shown to be promising candidates as antisense molecules (*7*, *8*). MMI dimers can be synthesized on a large scale and incorporated into oligonucleotides using automated procedures. Oligonucleotides containing MMI linkers are stable under physiological conditions. The studies in this laboratory and others indicate that MMI-containing oligonucleotides are resistant to cleavage by several nucleases that were tested. Furthermore, the phosphodiester (PO) within the MMI-PO-MMI trinucleotide linkage is also protected from nuclease digestion. Chimera oligonucleotides, such as those containing the MMI_i-PS_j-MMI_k (*i*, *j*, and *k* are number of internucleotide linkers) type of backbone modifications, are particularly attractive since these sequences remain as substrates of RNase H (*9*).

To further explore the applications of the MMI linker (i.e., logically programming the number and location of MMI in a sequence), it is critical to gain a fundamental understanding of the structural features and physicochemical properties of the MMI linker in single-stranded antisense oligonucleotides and in their hybrid duplexes with RNA sequences. A model compound, *N*,*N*-dimethylmethoxyamine (DMMA, Scheme 1), which is closely related to the MMI linker, has been studied via both experimental and theoretical approaches (*10*, *11*). DMMA has a pK_a of 3.7 (*12*), and thus, it is uncharged under physiological pH. As predicted by the gauche effect, DMMA prefers an anti conformation (Scheme 1) with the C3″−N−O−C5′ torsion angle being −120°. This conforma-

† This research was supported by NIH Grant R29GM59957 and the Robert A. Welch Foundation (Grant E-1270).

* To whom correspondence should be addressed. Telephone: (713) 743-2805. Fax: (713) 743-2709. E-mail: xgao@uh.edu.

‡ University of Houston.

§ ISIS Pharmaceuticals, Inc.

[1] Abbreviations: 1D, one-dimensional; 2D, two-dimensional; FMA, formacetal; 3′-TFMA, 3′-thioformacetal; COSY, correlation spectroscopy; DMMA, *N*,*N*-dimethylmethoxyamine; DQF, double quantum filtered; *g*, gauche; *t*, trans; MDS, molecular dynamics simulations; MMI, methylene methylimino; NMR, nuclear magnetic resonance; NOE, nuclear Overhauser effect; NOESY, nuclear Overhauser effect and exchange spectroscopy; rmsd, root-mean-square deviation; T_m, melting temperature; TOCSY, total correlation spectroscopy; UV, ultraviolet.

10.1021/bi990456x CCC: $18.00
Published on Web 09/09/1999

Scheme 1

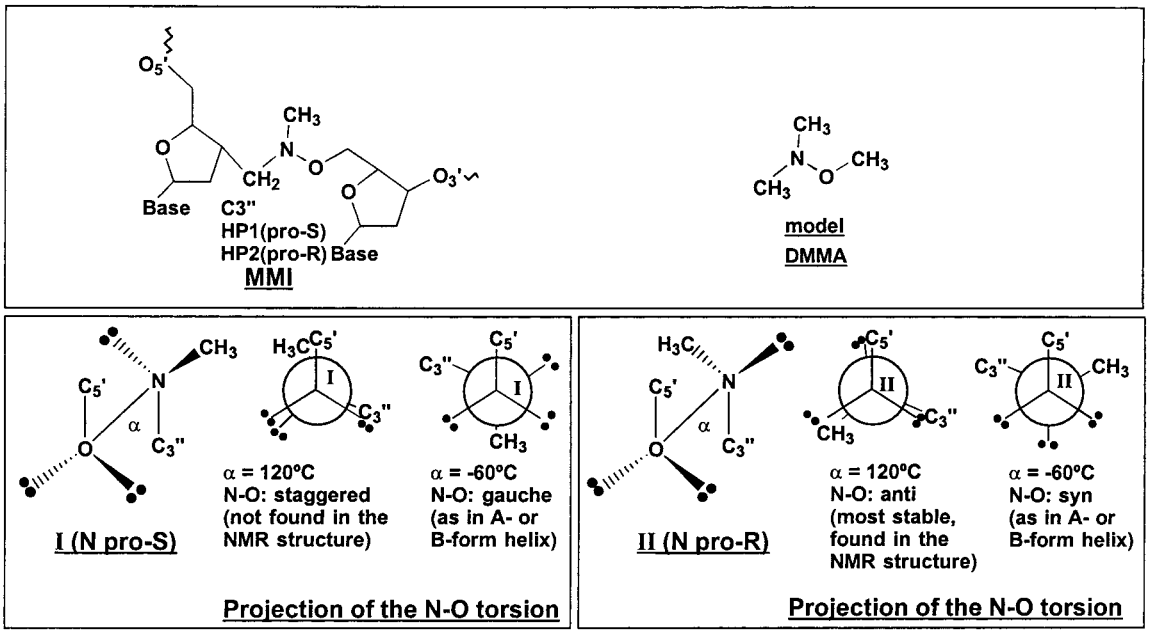

tion is stabilized by ~3 kJ/mol compared to other conformers. The isomerization between the two enantiomers due to the inversion of the pyramid N configuration is rapid and was not considered by these studies. A dinucleotide T1-MMI-T2 has been examined by NMR and molecular dynamics simulations (MDS) (*13*). In NMR spectra obtained in DMSO/CD_3OD, two conformations were detected at temperatures below −20 °C. In both forms, the conformations of the T1 sugar are mainly 3′-endo, while those of the T2 sugar are much less 3′-endo-like. Although not all NOEs related to the NMe group were entailed, the major form exhibited moderate NOEs from T2 H6 to the methylene protons of MMI and no NOE from T2 H6 to its own H5″. In contrast, the minor form exhibited NOEs between T2 H6 and its own H5″. These variations in NOE patterns are attributed to a $g+$ to t transition at the γ angle (O5′−C5′−C4′−C3′) of T2 in the minor form. MDS result in mainly one family of structures, which are characterized by a set of backbone torsion angles that are close to those of a canonical A-form helix. The NMe group was described as inverting between the "in" and "out" positions with marginal perturbations on backbone torsion angles. An FT-IR study of antisense oligonucleotide·RNA duplexes containing multiple substitutions of the MMI linker and 2′-OMe found a distinct C2′- to C3′-endo conformational transition induced by the modifications at consecutive residues and the resemblance of the duplex to an A-form helix (*14*).

The structural details of the MMI linker, however, have not been examined in the context of oligonucleotides, which are systems that are more relevant to biological applications compared to some discussed above. To improve our understanding of the structural role of this important backbone linker, several single-stranded MMI-containing dodecamers and their hybrid duplexes have been studied using high-resolution NMR, UV, and enzymatic digestion experiments in this laboratory. We report here the high-resolution structure of a hybrid duplex, d(CGCGTT-MMI-TTGCGC)·r(GCG-CAAAACGCG) or R4 (Scheme 2). The results of this structure study will be discussed with focuses on the features of the MMI backbone linker and the comparisons of R4 with other antisense duplexes studied in this laboratory, such as RII and RIII, hybrid duplexes containing a formacetal (FMA) and 3′-thioformacetal (TFMA) backbone linker, respectively, and RI, a hybrid duplex containing a natural phosphodiester backbone (Scheme 2) (*15*−*17*).

MATERIALS AND METHODS

Sample Preparation. The MMI linker was incorporated as a T-MMI-T dimer, which was synthesized as described previously (*8*). d(CGCGTT-MMI-TTGCGC) and r(GCG-CAAAACGCG) strands were synthesized and purified by R. T. Pon (University of Calgary, Calgary, AB). These samples were desalted on size-exclusion (Bio-Rad, PG-60) and sodium exchange (Aldrich, Dowex-50 H^+-form) columns eluted with H_2O. NMR samples were dissolved in 0.1 M NaCl, 10 mM sodium phosphate, and 0.1 mM sodium EDTA using D_2O (99.96%, Cambridge Isotopes, Inc.) and 90% H_2O/10% D_2O as solvents for the observation of nonexchangeable and exchangeable protons, respectively. The final NMR samples contained the duplexes at concentrations of 1−2 mM. The pH was 6.0−6.5.

Optical T_m Determination. The melting temperatures of R4 and its comparison hybrid duplex RI were measured in parallel using a 12-cell temperature variation UV spectrophotometer (Carry 3E, Varian). The solution conditions were the same as those used for NMR samples. Procedures of UV measurements and T_m derivations were as reported previously (*16*). The T_m values for R4 and RI are 47.7 ± 0.6 and 50.9 ± 0.2 °C, respectively.

NMR Experiments. All NMR experiments were conducted on a Bruker AMX-II 600 MHz spectrometer. Proton chemical shifts (Table S1) were referenced to the HOD resonance (4.70 ppm at 25 °C, temperature correction factor is −0.0109 ppm/°C). NMR data were processed using UXNMR (Bruker Instruments, Inc.) and FELIX v2.30 and v95 (Molecular Simulations, Inc.). The annealing of the modified DNA strand with the RNA strand was monitored by one-dimensional (1D)

Scheme 2

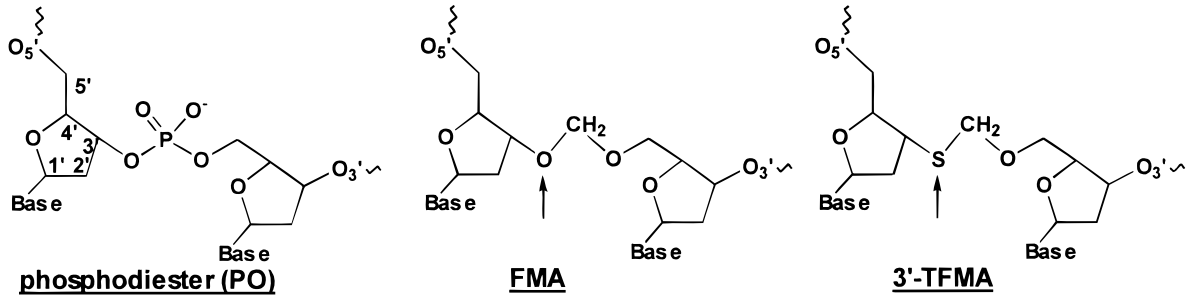

DNA:5'-	C1	G2	C3	G4	T5	T6	-X-	T7	T8	G9	C10	G11	C12
RNA:3'-	G112	C111	G110	C109	A108	A107		A106	A105	C104	G103	C102	G101

R4	X = MMI
RI	X = PO
RII	X = FMA
RIII	X = TFMA

proton spectra at room temperature. The final pH was determined from ^{31}P (phosphate salt, 10 mM) chemical shifts calibrated using a micro pH meter. Two-dimensional (2D) NOESY spectra of the exchangeable protons were acquired at 13 °C, with a 3 s relaxation delay, 50 and 140 ms mixing times, a 22.5 ppm spectral window, and 4096 × 512 data points. 2D NOESY spectra of nonexchangeable protons were acquired with a 4−5 s relaxation delay, 50, 100, and 250 ms mixing times, a 9 ppm spectral window, and 4096 × 512 data points, at 17 °C. NOESY spectra were used to trace through space connectivities and to obtain chemical shifts of all ^{1}H resonances. The final assignments were completed using a grid search of the FELIX cross-peak database files as described previously (*16*). Specific assignments of the linker region are discussed in the text. TOCSY (75 ms isotropic mixing time), DQF-COSY, and COSY-35 data were obtained with spectral parameters identical to those used for the nonexchangeable NOESY experiments. ^{31}P 1D and ^{1}H-detected ^{1}H−^{31}P COSY spectra were recorded at 17 and 25 °C, respectively. The sweep width was 3.33 ppm centered at the HOD resonance in the ^{1}H dimension (F_2) and 4.55 ppm centered at −3.39 ppm in the ^{31}P dimension (F_1). COSY-35 spectra were used to measure $J_{1'-2'}$ and $J_{1'-2''}$ on the basis of the separation (in hertz) between antiphase or in-phase multiplets along the resonance frequencies of H1′ protons, since the passive coupling components in these cross-peaks are suppressed. Accurate measurements of $J_{3'-2'}$, $J_{3'-2''}$, and $J_{3'-4'}$ were prohibited because the ambiguities from passive coupling were still too significant in these multiplets. However, qualitative analysis of the patterns and intensities of the cross-peaks due to H3′−H2′ ($I_{3'-2'}$), H3′−H2″ ($I_{3'-2''}$), and H3′−H4′ ($I_{3'-4'}$) couplings in COSY-35, DQF-COSY, and TOCSY spectra provided the relative J values for these spin pairs. Cross-peaks with greater intensity are associated with larger J coupling constants.

Dihedral Angle and Distance Restraints. A large number of sugar torsion angle restraints, such as υ_1 (torsion of C1′−C2′) and υ_3 (torsion of C3′−C4′) angles, were derived from sugar ring pseudorotation angles (*18*) based on scalar coupling constant analyses described above. Error bounds used in later structure calculations for these torsion angle restraints were ±10°. Except for the linker T6-T7, the backbone angles of R4 were estimated to be close to those of canonical duplexes (its ^{31}P resonances were narrowly distributed in a region of <0.6 ppm). The restraints for the RNA strand that was used were as follows [values (degrees) in parentheses were measured from an A-form duplex]: α, −88 ± 10 (−88); β, −149 ± 10 (−149); γ, 47 ± 10 (47); ϵ, 170 ± 10 (171); and ζ, −40 ± 10 (−44). The restraints for the DNA strand that was used were as follows (values in parentheses were measured from a B-form duplex): α, −65 ± 20 (−39); β, −149 ± 10 (−151); γ, 47 ± 10 (31); ϵ, 165 ± 20 (159); and ζ, −65 ± 30 (−99). Larger bounds (additional 10−20°) were added to those of the terminal residues. Distance restraints were derived from NOE assignments for nonexchangeable and exchangeable resonances. The cross-peak volumes from the three nonexchangeable proton NOESY spectra were converted to distances using MARDIGRAS (*19*) as described previously (*20*). Three sets of distance restraints were derived. These are the ones related to the MMI linker protons, the ones related to the modified T6 and T7 residues, and all other distance restraints. NOEs of exchangeable protons were used to define Watson−Crick base pairs. Since no cross-peaks were detected for the interstrand contacts between sugar protons, repulsive distance restraints were applied at a later stage of structure calculation to separate these protons by greater than 5.5 Å to prevent the minor groove from collapsing.

Structure Calculations. Structure calculations were performed using XPLOR (*21*). The initial structures were

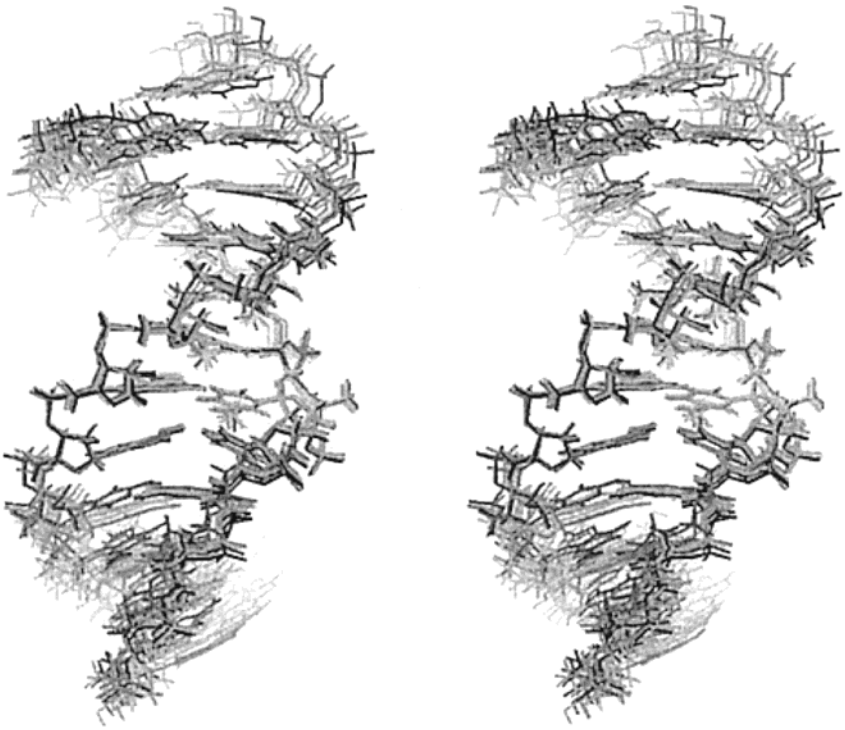

FIGURE 1: Overlayed structures of the R4 duplex. Six structures are shown in stereoview. Only non-hydrogen atoms are displayed for clarity.

obtained by free MDS of ideal A- and B-form duplexes generated from QUANTA. This process was initiated by assigning each structure a randomly chosen seed number, which sets the velocity for MDS. Fifty randomized initial structures were generated, 25 from the A-form and 25 from the B-form, and their coordinate rmsd was larger than 3.5 Å. The MMI linker was built into the molecule using the Molecular Editor in QUANTA. The corresponding parameters were from the DMMA study (*10*) and/or from the QUANTA data library. NOE force constants of 20−40 kcal mol^{-1} $Å^{-2}$ were assigned to the three groups of distance restraints to give the most important and well-resolved restraints the most weight. Most of these are related to the linker protons or to the protons of the T6 and T7 residues. A typical MDS process using NMR distance and dihedral angle restraints involved Powell energy minimization of the input structures for 200 steps (no restraints applied); Verlet MDS (distance restraints applied), including heating and scaleup NOE force constants, equilibration at elevated temperatures, and cooling steps; and final energy minimization using both distance and dihedral angle restraints. A detailed description of the calculation strategies that were used has been presented previously (*17*). For each iteration, the calculated distances and dihedral angles were compared with not only the input restraint files but also the original NMR spectra. These comparisons allowed error corrections and addition of newly assigned restraints.

The final six structures of R4 exhibit satisfactory coordinate convergence (Figure 1), bonding geometry, low nonbonding energies, and a good agreement with the experimental data. These results are summarized in Table 1, and the detailed comparisons of the consistency in linker-related NOEs are given in Figure 2 and Table S2. The structural parameters, such as those characterizing the correct chirality, the helical geometry, and the relative orientations of each residue, were analyzed using XPLOR and CURVES (*22*). Structures were displayed and visually analyzed using QUANTA.

Table 1: Summary of the R4 Structure Calculation Results[a]

rmsd of coordinates[b] (Å)	
all residues	
all atoms	0.62 ± 0.13
non-hydrogen atoms	0.56 ± 0.11
central six residues	
all atoms	0.38 ± 0.06
non-hydrogen atoms	0.32 ± 0.04
ideal geometry	
total *E* (kJ/mol)	−5.1
bond (Å) (832)	0.0159 ± 0.0002
angle (deg) (1496)	3.00 ± 0.18
NOE restraints (Å)[c]	
NOE (all) (411)	0.24 ± 0.01
NOE (MMI) (28)	0.25 ± 0.01
NOE (T6 and T7) (63)	0.23 ± 0.03

[a] Parameters were measured from the final six structures. [b] These are values of comparison with an averaged structure. [c] Numbers in parentheses are the total number of restraints.

Coordinates. The coordinates of the reported structures of R4 have been deposited at the Brookhaven Protein Data Bank (accession number 1CX5).

RESULTS AND DISCUSSION

^{1}H Assignments of R4 (Excluding Linker Protons). A set of 2D NMR spectra of R4 have been recorded and analyzed as described previously (*16*). NOEs due to base to H1′ sequential connectivities are shown in Figure 3. ^{1}H exchangeable and nonexchangeable resonances were assigned to near completion except for H5′ and H5″ of the unmodified sugar residues (Tables S1A and S1B) (*20*). Chemical shift comparisons between the non-linker-related residues of R4 and their counterparts in the unmodified RI revealed (Table S1C)

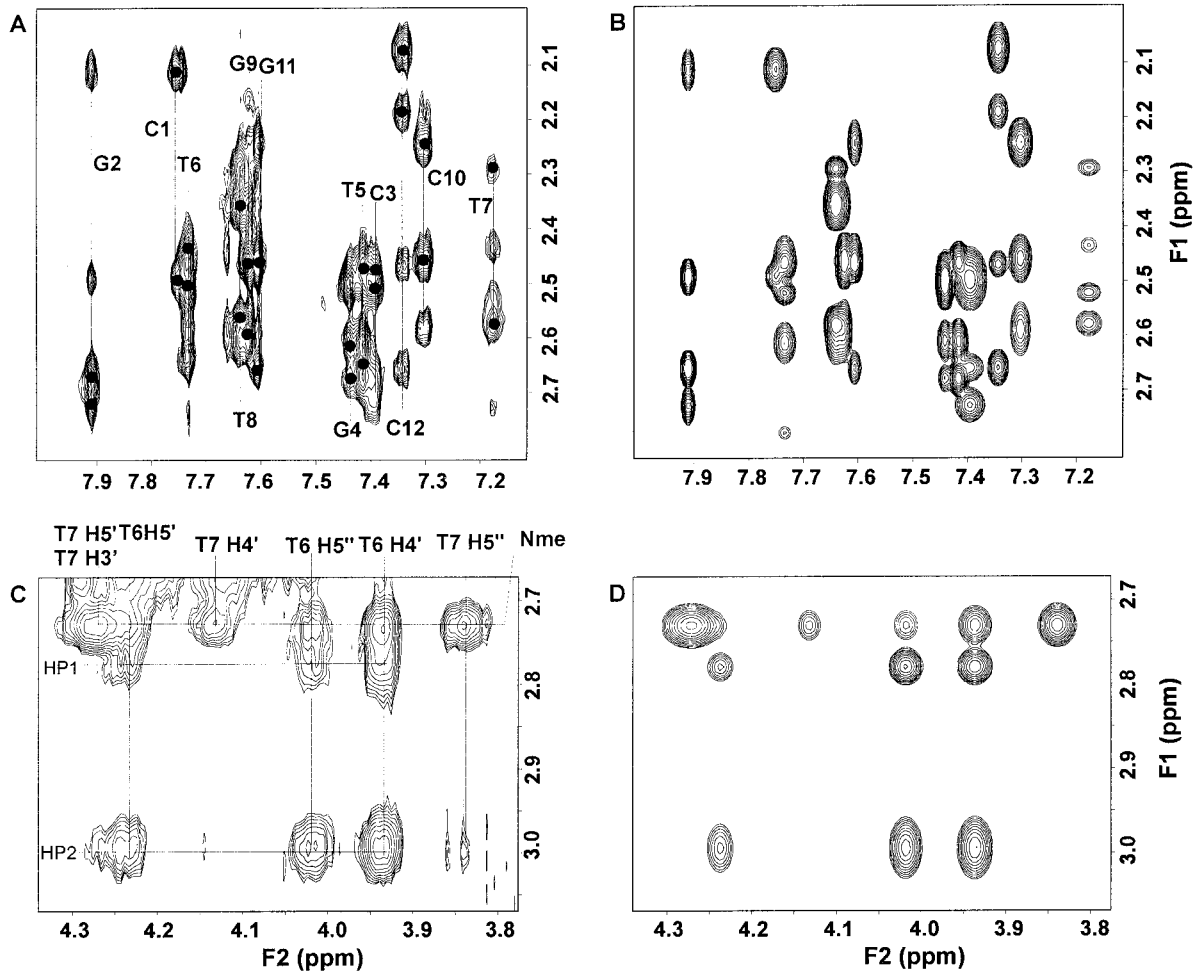

FIGURE 2: Expanded NOESY spectra (250 ms mixing time) of the R4 duplex. Panels A and C depict experimental data, and panels B and C depict back-calculated spectra. (A and B) NOE connectivities from the base proton (F_2 axis) to sugar H2′ and H2″ proton resonances (F_1 axis). Residue numbers are placed next to the solid lines corresponding to chemical shifts of base protons. Intraresidue NOEs are marked with solid balls. (C and D) NOEs related to the MMI linker protons (F_1 axis) to T6 and T7 sugar protons (F_2 axis).

(*20*) that the structural adjustments that occurred at the MMI linker site are mostly localized with a few exceptions as discussed later. Comparisons of sequential NOE connectivities of R4 (i.e., NOEs of base to sugar protons, partly shown in Figure 3) with those found in other backbone-modified antisense duplexes, such as RIII (*16*), were made. These results reveal that these NOEs follow a similar relative intensity pattern, indicating an overall comparable structural configuration of the antisense duplexes containing a single backbone modification. ^{31}P resonances, recorded in the 1D and the ^{1}H-correlated 2D spectra, appear within a narrow range of 0.6 ppm (*20*), indicating that the canonical backbone conformation of the duplex, with the exception of the linker, is not particularly perturbed.

NMR Spectral Analysis of the Linker Region of R4. The residues located near the modification site, in either the RNA or the DNA strand, exhibit spectral features that are indicative of stronger effects of the MMI group on the local structure than those observed in other modified hybrid duplexes. For instance, the NOEs connecting the H1′ with the base protons of residues T7, A105, A106, A107, and A108 and at the steps of T6-T7, A105-A106, and A106-A107 are much weaker in R4 (Figure 3). These NOEs, however, can be detected in an NOESY spectrum recorded using a longer mixing time (500 ms). Their counterparts are well-defined in the unmodified RI and the modified RII (T6-OCH_2O-T7) and RIII (T6-SCH_2O-T7) (*15*, *16*). The weakening of these NOEs in R4 is not, however, due to a major disruption of the A·T base pairs, since NOEs involving the base-paired T imino protons and the A H2 to cross-strand H1′ are well-defined in the corresponding 2D NOESY spectra. Thus, because the helix of R4 remains intact, while H1′ sequential connectivities become weaker, the structural details of the MMI linker may be different from what was observed for the analogous RI, RII, and RIII hybrid duplexes.

Distinct spectral features associated with the MMI linker are also evident in the COSY (COSY-35, DQF-COSY, and TOCSY) spectra. The *J* coupling cross-peaks of the sugar protons of the T6 and T7 residues exhibit different patterns compared to those of other DNA sugar rings. $J_{1',2''} > J_{1',2'} \sim 0$, and/or strong $J_{3',4'}$ values were observed for the T6 and T7 residues (*20*), indicating that these MMI-linked residues contain typical C3′-endo sugar puckers. In comparison, RII (T6-OCH_2O-T7) exhibits typical C2′-endo and RIII (T6-SCH_2O-T7) more C3′-endo characteristics for only the T6 sugar. The T7 sugars in RII and RIII do not appear to be affected as much by the backbone modifications as shown in the MMI-modified R4. This observation of sugar pucker conformation again illustrates the very different nature of the MMI linker compared to the linkers of the formacetal series.

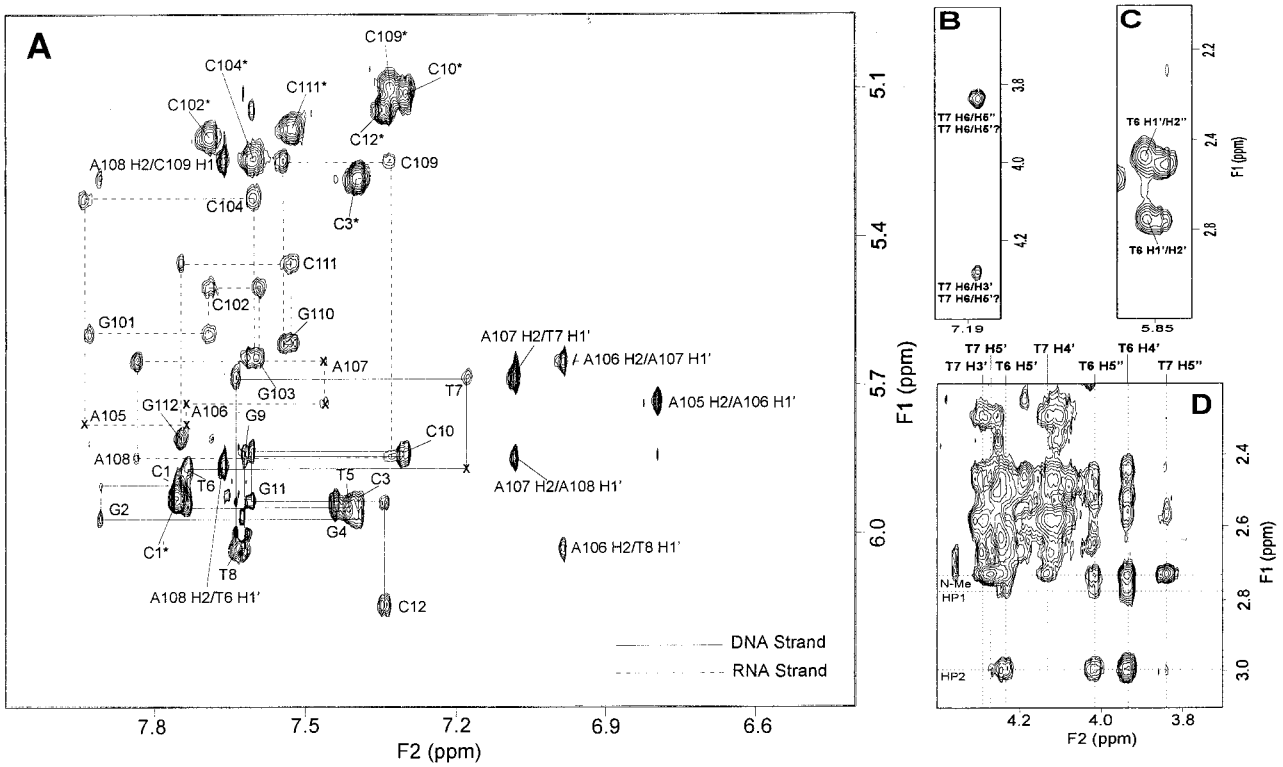

FIGURE 3: Expanded NOESY spectra (A and D, 250 ms mixing time; and B and C, 100 ms mixing time) of the R4 duplex. (A) NOE connectivities from the base proton (F_2 axis) to sugar H1′ and base H5 protons (F_1 axis). Residue numbers indicate intraresidue NOEs, and sequential connectivities are connected by solid or dashed lines for the DNA or the RNA strand, respectively. C H5 and C H6 NOEs are labeled with asterisks. (B) An NOE between T7 H6 (F_2 axis) and T 7 H5″ (F_1 axis). (C) NOEs from T6 H1′ (F_2 axis) and T6 H2′ and H2″ (F_1 axis). (D) NOEs from the sugar H3′, H4′, H5′, and H5″ protons of the T6 and T7 residues (F_2 axis) to the MMI linker NMe and methylene HP1 (*pro-S*) and HP2 (*pro-R*) protons (F_1 axis).

The three ^{1}H resonances of the MMI moiety (Figure 4A) were unambiguously identified, which are NMe at 2.73 ppm and the methylene HP1 and HP2 at 2.77 and 2.99 ppm, respectively. These resonances exhibited distinct NOE peak patterns and chemical shift positions, which are easily distinguished from those of nucleic acid resonances. For instance, HP1 and HP2 were differentiated from sugar H2′ and H2″ methylene protons, since these protons did not exhibit typical sugar proton connectivities and HP2 (HP1 is too close to NMe protons) also exhibited a strong NOE to NMe due to the close vicinity of the two protons (Scheme 1). These assignments of the linker protons were also confirmed in the studies of an R5 hybrid duplex containing [^{13}C]NMe MMI groups (*20*). A number of NOEs (Figures 2 and 3, and Table S2) between the MMI linker and other R4 protons were assigned.

The information pertinent to the linker NOEs and their relative intensities are particularly important for the delineation of the orientation of the linker. All linker protons are most close to T6 H4′ (3.94 ppm) (Figure 2A). One (2.99 ppm) of the two methylene protons is closer to T6 H5″ (4.02 ppm) than T6 H5′ (4.24 ppm) or H3′ (2.52 ppm). The NMe group is weakly linked to T7 H5′/H5″ (4.28 ppm). The NOEs from the linker protons to the base and H1′ protons of T6 and T7 are extremely weak, observed as minor peaks only in the 250 ms mixing time NOESY spectrum. The NOEs from the linker protons to T6 H3′, H2′, and H2″ (2.52, 2.57, and 2.44 ppm, respectively) are also weak. However, several lines of evidence indicate that T6 sugar H2′ and H2″ may be mobile, since the geminal scalar coupling ($J_{H2',H2''} > 10$ Hz) between the two protons gave rise to only a weak cross-peak. Additionally, these T6 resonances and T6 H3′ have broad line widths. Given the fact that the distances from HP1 and HP2 to T6 H3′ are determined by covalent bonds, their weak NOEs are consistent with a T6 sugar that may be conformationally flexible. Additionally, NOEs exhibit that the γ angle of T7 is not likely to be $g+$ as it is in a canonical duplex, since NOEs were found between T7 base H6 and H5′ and H5″. On the other hand, the γ angle of T6 is likely to be $g+$, since no NOEs were found between base H6 and H5′ and H5″. These lines of spectral evidence qualitatively place the NMe group away from the inner helix and provide definitions for the local conformation of the MMI linker.

Structure Refinement of R4. Complete NMR spectral analyses generated a large number of restraints that permit high-resolution structure elucidation of the R4 hybrid duplex. For structure refinement, we used MARDIGRAS (*19*) and XPLOR (*21*) and a total of 411 distance restraints (346 nonexchangeable proton pairs and 64 Watson−Crick base pair restraints) and 150 dihedral angle restraints. Twenty-eight NOEs and two dihedral angles were used for the linker, and 63 NOEs and 13 dihedral angles were used for T6 and T7 residues. The T6 ϵ angle was derived from NOEs connecting HP1 and HP2 to T6 sugar protons and was restrained in the range of $75 \pm 25°$. The T7 γ angle was derived from NOEs from T7 H6 to T7 H5″ and was restrained in the range of $120 \pm 60°$. The computational statistics of the final six structures are summarized in Table 1. The six structures are low-energy forms and show good agreement with the experimental data (Figure 2 and Table S2). These structures have been characterized by standard helical parameters, such as glycosidic and phase angles,

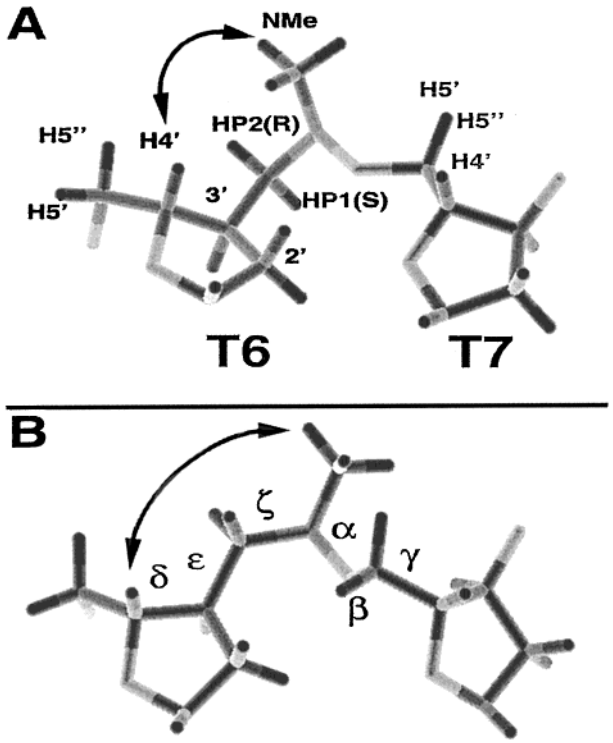

FIGURE 4: Drawings of MMI in (A) one of the NMR refined structures and (B) a model A-form. The names of the MMI protons and the backbone torsion angles at the modification site are included. The arrow in panel A denotes the closely related NMe and the T6 H4′ protons.

backbone torsion angles, and intra- and interbase orientations, determined using XPLOR and CURVES (*22*) (Table S3).

Structure and Structural Comparisons of the R4 Duplex. The stereoview of a representative structure of R4 is displayed in Figure 5A. The overall structural features of R4 are mixed B- and A-form with the latter dominating the helical geometry (Table S3 and Figure S1). This is similar to what was observed for the unmodified RI duplex (*15*) and the RIII hybrid duplex containing a 3′-TFMA between T6 and T7 (Scheme 2) (*15*−*17*). An overlay of the two RNA strands of RIII and R4 demonstrates the overall similarity between the structures of the RNA strands as well as deviations of local structures of R4 from those of RIII (rmsd $\sim$ 1.7 Å) (Figure 5B). The slightly extended A_4 tract of R4 may be responsible for the reduction in the inter-residue base proton to H1′ NOEs. Two helical parameters are characteristic of an A-form structure: the x-displacement (D_x) (A-form value of −5.3 Å and B-form value of 0.6 Å) and the inclination (η) (A-form value of 19.5° and B-form value of −4.6°). For R4 (only nonterminal residues are considered), the MMI-modified DNA strand has D_x and η in the ranges of −2.8 to −4.1 Å and 2−22°, respectively; the duplex has D_x and η in the ranges of −3.0 to −3.8 Å and −2.5−12.9°, respectively (residues close to the 3′-end exhibit η values of −2.5 and −1.7°). These values clearly reflect an A-form-like structure with negative D_x and mostly positive η values. The separation between the base pairs of R4 is 3.0 Å compared to the 2.3 Å separation of A-form and the 3.4 Å separation of B-form. Therefore, the length of the helix is hybrid in nature. Sugar pucker conformations also contain hybrid features with some of the DNA strand residues (G2, C3, T8, C10, and G11) in the C2′-endo family, G4 and T5 in intermediate C2′- and C3′-endo conformations (the linker residues will be discussed separately), and the RNA strand in the C3′-endo conformation. The analyses of these general features reveal that the structural changes of the residues distant from the MMI linker are minimal. This assessment agrees with the observed minor chemical shift perturbations of the relevant protons of R4 compared to those of RI. However, one apparent exception can be found at the kink that occurred between the T8 and G9 residues (Figure 5C). This may be due to slightly decreased α (−87° compared to −77° for T8 and C10) and γ (43° compared to 64° and 53° for T8 and C10) angles of the G9 residue. Since this structural feature was not observed in other analogous hybrid duplexes, such as RIII (*16*), the observed backbone perturbation may be attributed to the presence of the MMI linker, which requires different geometry arrangements due to its neutral charge state and shorter covalent bond lengths compared to the natural phosphodiester in RI and the 3′-thioformacetal modification in RIII (*15*−*17*).

Structural Refinement of the MMI Linker. Linker structural variables were carefully examined during the MDS structure refinement. In these calculations, no backbone angle restraints were applied to T6 ζ, T7 α, and β angles and only loose H-bond restraints (error bounds were 0.2−0.7 Å) applied to the T6·A107 and T7·A106 base pairs. This resulted in a set of structures which agreed well with NMR restraints and have low empirical potential energies. On the basis of these structures and the NOE data, the stereochemistry of HP1 (pro S, 2.77 ppm) and HP2 (pro R, 2.99 ppm) and T6 H5′ (4.24 ppm) and H5″ (4.02 ppm) was analyzed. Each of these protons was then stereospecifically assigned. NOE and dihedral angle restraints were updated accordingly. Structure refinement was continued to give a new set of structures that converged at T6 (ϵ = 84° and ζ = 38°) and T7 (α = 132°, β = 177°, and γ = 158°). The N−O torsion of the MMI linker is anti with NMe in a pseudo-R conformation (Scheme 1 and Figure 4).

Although these calculated structures of the MMI linker in R4 are lower-energy forms and agree well with the experimental data (Figure 2 and Table S2), other possible structures were sought for completeness. Three sets of further structure refinement calculations were performed: (**a**) inverted the chirality of the NMe group and refined the structures using the same set of restraints used previously; (**b**) defined ϵ as 160 ± 20 (an alternative conformation based on NMR data), removed NOE restraints related to HP1 and HP2, and refined as described previously; and (**c**) defined the backbone angles between T6 and T7 in the range found in canonical A- and B-form helices, removed NOE restraints related to HP1 and HP2, and refined as described previously. Refinement **a** was performed to investigate whether it was possible for the NMe group to flip between the two isomeric forms; refinement **b** was performed to seek alternative conformations that can potentially fit the NOEs correlating HP1 and HP2 with T6 H4′ (given a fixed sugar conformation, the separations among these protons are determined by the ϵ angle), and refinement **c** was performed to ask the question of whether it was possible to confine the MMI linker in a conformation similar to a regular helix. Refinement **a** essentially returned structures that were consistent with the first set of structures. Therefore, the NMe group prefers to be present in predominately one configuration and the inversion energy barrier for this group

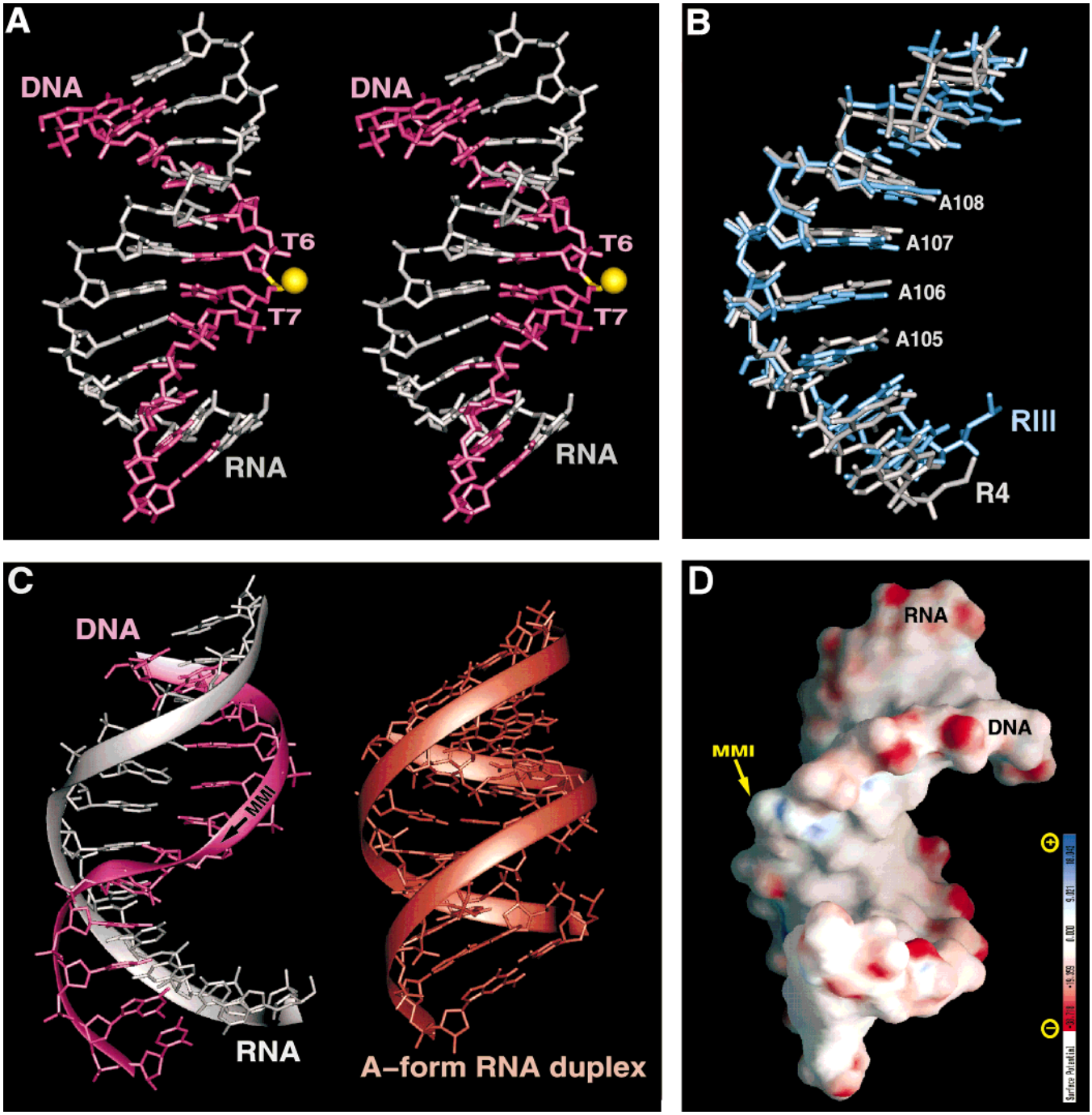

FIGURE 5: Structure of the R4 duplex. (A) Stereodrawing of a representative R4 duplex from the final six structures. DNA and RNA strands are magenta and light gray, respectively. The MMI NMe is highlighted in yellow and shown as a van der Waals sphere (half of the full radius). (B) The overlay of the RNA strand in the hybrid duplexes containing a modified T6-T7 site. R3 contains a 3′-thioformacetal linker, and R4 contains an MMI linker (see Scheme 1 for chemical structures). The central A_4 tract is shown. (C) Comparison of the overall structural features of R4 with a canonical A-form RNA duplex. Ribbon drawings show the disruption in the helical transition of the DNA strand of the R4 duplex at the 3′-neighboring site of the MMI linker. (D) Electrostatic surface drawing of R4 generated using GRASP. Red and blue colors mark negative and positive charges, respectively. The backbone electron neutrality introduced by the MMI modification (close to a white color) is denoted by an arrow.

may be increased from <1 to ~4 kJ/mol (estimated K_{eq} of <0.05). Refinement **b** resulted in a set of diverse, low-quality structures where the NOE agreement was unacceptable. Refinement **c** generated only two distorted structures, and all other calculations were aborted abnormally, indicating conflicting energy terms if the MMI linker existed in an A- or B-form type of structure. Therefore, the structures described here are those derived from refinement a and the further refinement of the initial set of structures.

Structural Features of the MMI Linker. (a) Surface Orientation and Torsion Angles of the Linker. The exposed orientation of the MMI linker at the surface of the R4 duplex is displayed in Figures 4A and 5A. The backbone angles connecting T6 and T7 (ϵ, ζ, α, β, and γ, Scheme 1) are plotted in Figure 6. Important NOEs, which define the linker conformation, are those involving the NMe group. This group is closest to T6 H4′, close to T7 H5′ and H5″, and distant from other protons of the T6 and T7 residues. To accom-

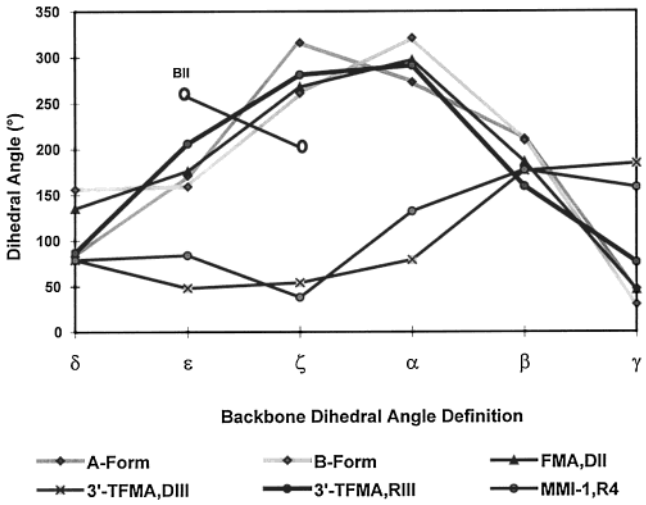

FIGURE 6: Summary of the backbone torsion angles at the modification site in various duplexes containing antisense oligonucleotide strands. All duplexes contain the same base composition, CGCGTT*TTGCGC and GCGCAAAACGCG, while the modification is located at the position marked with an asterisk. A- and B-form are canonical RNA·RNA and DNA·DNA duplexes. FMA, DII is the duplex containing a formacetal linker strand that hybridizes to a DNA complementary strand. 3′-TFMA, DIII is the duplex, and 3′-TFMA, RIII is the hybrid duplex, each containing a 3′-thioformacetal linker that hybridizes to a DNA or an RNA complementary strand, respectively. MMI-1 represents the R4 duplex. The plotted values were derived using XPLOR.

modate these NOEs, the MMI methylene group, which is located between NME and T6 H4′ (Figure 4), has to rotate in a way so that NMe and T6 H4′ can be less than 3.5 Å apart. This adjustment (compared to an A-form) is achieved at the T6 residue of R4 by a reduction in the ϵ angle from 175 to 84°, and an increase in the ζ angle from −45 to 38° (Figures 4 and 5). The changes in the ϵ and ζ angles are offset by the changes in the α and γ angles of T7 (Figure 6) so that the overall helicity of the duplex remains constant. The largely varied backbone angles between T6 and T7 correlate well with a few aberrant chemical shifts. For instance, the T6 H2′ and H2″ are inverted in their resonance frequencies (H2′ is downfield shifted compared to H2″), and T7 H3′ (4.28 ppm, confirmed by COSY peak assignments) is upfield shifted compared to that (4.81 ppm) in unmodified RI. Inspection of the structure of R4 and that of a model A-form (Figure 4) indicates that T6 H2′ becomes closer to T5 O5′ and that T7 H3′ becomes closer to its own H5′ and H5″ and farther away from T7 O5′ and phosphate oxygen atoms in R4. The electron inductive effect of the electron negative oxygen atom shifts the resonance frequencies of the nearby H to downfield, while moving away from these oxygen atoms results in upfield shifts. Thus, the described changes in the spatial relationships of the pertinent Hs are consistent with the observed chemical shift variations of T6 H2′ and T7 H3′ in R4. Another potential chemical shift−structure correlation is that since the T7 γ angle is anti, the upfield-shifted T7 H3′ may be diagnostic of this unusual backbone angle.

(b) Torsion Angle Comparisons with Other Antisense Duplexes. In Figure 6, the backbone torsion angles of the chemically modified sites in several antisense duplexes (*25*) are displayed. The figure compares RNA·DNA hybrid duplexes and DNA·DNA duplexes, RIII, R4, DII, and DIII. These sequences contain a T6-SCH_2O5′-T7 (3′-TFMA), a T6-$CH_2N(CH_3)$O5′-T7 (MMI), and a T6-OCH_2O5′-T7 (FMA) (Scheme 2). These backbone torsion angles are also compared with those of standard B- and A-form duplexes generated using QUANTA. Among these backbone parameters, those of RIII (*16*) and R4 were elucidated using the NMR computation method and those of DII (*23*) and DIII (*24*) were derived from a combination of modeling and qualitative NMR refinement. This comparison indicates that the torsion angles of R4 and DIII are strikingly similar and the conformations of both duplexes drastically deviate from canonical conformations. It is interesting to note that both R4 and DIII sequences form stable duplexes, having T_m values merely 3−4 °C lower than those of their counterpart unmodified duplexes. Similar T_m reduction has been observed in other backbone-modified duplexes without much backbone distortion (*16*). Thus, the backbone torsion angles adopted by R4 and DIII may represent an acceptable, alternative backbone conformation that may be accommodated in a right-handed helical duplex. Further structure studies should be accumulated to testify this point.

(c) Comparison of the MMI Linker in Different Sequences. The conformation of the MMI linker is more stable in R4 than that observed in the T1-MMI-T2 dimer, where isomerization coalesce of the NMe NMR signal in either an *R* or an *S* configuration was observed at 5 °C (*13*). The backbone conformations in the two sequences (R4 and the dimer) are distinctly different [e.g., T7(R4) $\alpha = 120°$ and T1(dimer) $\alpha = -120°$]. The conformational preferences of the MMI linker in a duplex versus those in a single-stranded dimer demonstrate the influence of several inter-related factors, such as overall flexibility allowed by the molecule and the energy requirement of the local chemical moieties and overall molecules, in the determination of the local structures of oligonucleotides. The understanding of the interplay of these and several other factors (*25*) is an important step toward the improved design of antisense sequences.

(d) Molecular Basis for the Conformation Adopted by the MMI Linker. Viewing of the structure of R4 indicates that the MMI linker adds a hydrophobic patch onto the otherwise negatively charged backbone with the methylene and the NMe groups aligning on the surface to join T6 H4′, H5′, and H5″ on one end and T7 H5′, H5″, and H4′ on the other end (Figure 5D). Two factors may account for the surface orientation of the MMI linker. One is steric. If the NMe group projected inward toward the helical axis, there would be severe clashes with the sugar ring of T6 and the C5′ group of T7. Second is bond angle energy. The stability of the linker is achieved by an anti conformation around the N−O bond, which is the most stable conformation found in the model compound DMMA (Scheme 1), if the gauche effect is taken into consideration. In contrast, if the backbone were to adopt a conformation typical of A-form, the N−O torsion would be in the unstable syn forms (Scheme 1). These forms encounter two unpaired electron repulsion interactions (when NMe is pseudo-*R*) or one of these interactions (when NMe is pseudo-*S*) (Scheme 1). It appears that in R4, the inherent stability requirement of the MMI group outweighs the backbone conformational preferences. The analogy that a backbone modification dominates the resultant local structure has been observed in the duplexes containing the FMA and the 3′-TFMA linkers (*15*−*17*, *25*). The presence of the MMI

linker, however, also introduces local motions that can be discerned at the T6 H2′, H2″, and H3′ protons. For instance, these protons give rise to weak, broad NOE cross-peaks to MMI HP1 and HP2. These data are not compatible with their fixed distances defined by chemical bond connections. At the present time, the exact nature of the local motions involving the T6 sugar is unclear. The structure adopted by the MMI linker is expected to significantly alter the surface properties, such as ion association and hydration, of the helix. Consequently, the basic properties of the duplex and their interactions with other molecules should be affected. An investigation in which such effects are examined in the current applications of the MMI-modified oligonucleotides should be of direct biological interest.

(e) An Analysis of C3′-Modified Oligonucleotide Sequences. There has been a rapid increase in the number of structures determined for DNA·RNA and antisense sequence·RNA hybrid duplexes (*16*, *25*−*30*). Several examples of C3′ modifications on the 2′-deoxyribose by a methylene group, such as C3′-CH_2 phosphonate (*26*) and C3′-CH_2CH_2NH (*28*), have demonstrated a 3′-endo conformation for the corresponding sugar moiety. The T6 sugar containing a C3′-MMI linker also adopts a typical C3′-endo pucker. The question is what is the molecular basis for this common feature of the C3′-CH_2 substitution. Recognizing that the C3′ modifications described above vary in chemical structures but all contain a C3′-CH_2 group, we have recorded the statistics of the interproton distances between those of the C3′-CH_2 group (equivalent to HP1 and HP2) and the sugar moiety (most relevant protons include H2′, H2″, H3′, and H4′) at variant ϵ angles (Table S4). Interestingly, for a given ϵ angle, the average interproton distance is consistently shorter in the C3′-endo sugar than in the C2′-endo sugar. Furthermore, the steric clash as represented by the shortest interproton distances is always more severe in the C2′-endo sugar than in the C3′-endo sugar. When these facts are taken together, qualitatively, the tendency to form 3′-endo sugar rings driven by a C3′-CH_2 substitution may be attributed to a more favorable balance of van der Waals forces in this conformation than in the C2′-endo sugar pucker.

(f) Long-Range Effect of the MMI Linker. Moreover, MMI extends its influence to the sugar moiety of the distantly related residue, T7, inducing its formation of a C3′-endo pucker. This effect was not observed in any of the above-mentioned backbone modifications. Conceivably, a homogeneous DNA helix containing sugars in a C3′-endo conformation can be achieved through multiple MMI modification. Such a structural homogeneity achieved in the MMI-modified sequences should improve the stability of the corresponding hybrid duplexes. It has been recognized that local and global structures are important elements for nucleic acid recognition, and for this very reason, we believe that the structural variations induced by MMI would render the MMI-containing sequences unrecognizable by cellular nuclease as substrate for cleavage. Indeed, in the MMI stand of R4, we observed an increased level of protection of the PO linkages adjacent to the MMI linkages in nuclease digestion experiments, which will be reported elsewhere.

CONCLUSIONS

Replacement of a phosphodiester with an MMI group in a DNA strand converts a smaller, negatively charged, polar chemical moiety into a larger, neutral, lipophilic one. This study is mostly interested in the impact of such a backbone modification on the solution structures and, hence, the solution properties of the modified duplexes. Our NMR analyses and structure elucidation reveal the helical surface arrangement of the MMI-modified duplex that accounts for the increased lipophilicity and, thus, better cell permeability of the MMI-modified antisense sequences. The MMI backbone linkage is associated with a strong preference for C3′-endo sugar pucker for residues on either side of the modification and drastic backbone structural changes. The adoption of predominant C3′-endo sugar pucker at the residues of the modification site promotes A-form features of the duplex. Therefore, these structural variations may be more compatible with RNA target strands than other modified antisense oligonucleotides which features more DNA strand characteristics. Furthermore, the incorporation of an MMI linker into a T·T step in an oligonucleotide sequence induces characteristic structural changes which, in many aspects, are much more pronounced, in the residues that are affected and the extent of changes, than those observed in the comparison antisense duplexes (RII and RIII) containing a modified backbone linker (Scheme 2).

Structural analysis of the MMI linker in R4 and its comparisons with the TFMA and the FMA linkers reveals a new family of low-energy helical conformations that are likely to be accommodated in stable duplexes. These studies also reveal synergies of various factors which influence the end results of chemical modification of antisense sequences. Thus, it is clear that for any promising modification, the requirements are its compatibility with the local and global structures and its ability to form a conformation that can be accommodated in the helix with minimal energy costs. This is in addition to what has been discussed here and in many literature articles about favorable molecular forces that govern the formation of stable structures. The given environment has to be considered. One aspect of our further studies will be an examination of the effects of multiple substitutions on duplex structures and stabilities and modification effects on the preorganization of single-stranded antisense sequences. The understanding of these aspects should help broaden our views on the factors, which contribute to better antisense oligonucleotides and have far reaching implications in the development of effective antisense therapeutics.

ACKNOWLEDGMENT

We thank Ms. Laëtitia Sonigo for generating Table S4. The 600 MHz NMR spectrometer at the University of Houston is funded by the W. M. Keck Foundation. Acknowledgment is made to the Institute of Molecular Design and the W. M. Keck Center for Computational Biology at the University of Houston for computer resource support.

SUPPORTING INFORMATION AVAILABLE

Structural data for compounds used in this study. This material is available free of charge via the Internet at http://pubs.acs.org.

REFERENCES

1. Zamecnik, P. C., and Stephenson, M. L. (1978) *Proc. Natl. Acad. Sci. U.S.A. 75*, 280−284.

2. Crooke, S. T. (1997) *Adv. Pharmacol. 40*, 2−49.
3. Agrawal, S., and Iyer, R. P. (1995) *Curr. Opin. Biotechnol. 6*, 12−19.
4. Uhlmann, E., and Peyman, A. (1990) *Chem. Rev. 90*, 544−584.
5. Sanghvi, Y. S. (1998) in *Comprehensive natural products chemistry* (Barton, D. H. R., and Nakanishi, K., Eds.) Vol. 7, Pergamon Press, New York.
6. Marshall, W. S., and Caruthers, M. H. (1993) *Science 259*, 1564−1570.
7. Vasseur, J. J., Debart, F., Sanghvi, Y. S., and Cook, P. D. (1992) *J. Am. Chem. Soc. 114*, 4006−4007.
8. Morvan, F., Sanghvi, Y. S., Perbost, M., Vasseur, J.-J., and Bellon, L. (1996) *J. Am. Chem. Soc. 118*, 255−256.
9. Sanghvi, Y. S., Swayze, E. E., Peoc'h, D., Bhat, B., and Dimock, S. (1997) *Nucleosides Nucleotides 16*, 907−916.
10. Rankin, D. W., and Todd, M. R. (1981) *J. Mol. Struct. 71*, 171−183.
11. Radom, L., Hehre, W. J., and Pople, J. A. (1972) *J. Am. Chem. Soc. 94*, 2371−2381.
12. Bissot, T. C., Parry, R. W., and Cambell, D. H. (1957) *J. Am. Chem. Soc. 79*, 796−800.
13. Mohan, V., Griffey, R. H., and Davis, D. R. (1995) *Tetrahedron 51*, 8655−8668.
14. Gousset, H., Liquier, J., Tailandier, E., Sanghvi, Y. S., and Peoc'h, D. (1998) *J. Biomol. Struct. Dyn. 15*, 931−936.
15. Gao, X., and Jeffs, P. W. (1994) *J. Biomol. NMR 4*, 367−384.
16. Rice, J. S., and Gao, X. (1997) *Biochemistry 36*, 399−411.
17. Cross, C. W., Rice, J. S., and Gao, X. (1997) *Biochemistry 36*, 4096−4107.
18. Saenger, W. (1984) *Principles of Nucleic Acid Structure*, pp 14−20, Springer-Verlag, New York.
19. Schmitz, U., and James, T. (1995) *Methods Enzymol. 261*, 3−44.
20. Yang, X. (1998) Conformational and structural studies of antisense oligonucleotides by nuclear magnetic resonance spectroscopy, Ph.D. Dissertation, University of Houston, Houston, TX (Chapter IV).
21. Brunger, A. T. (1992) *Xplor Manual V3.0*, Yale University Press, New Haven, CT.
22. Lavery, R., and Sklenar, H. (1988) *J. Biomol. Struct. Dyn. 6*, 63−91.
23. Veal, J. M., Gao, X., and Brown, F. K. (1993) *J. Am. Chem. Soc. 115*, 7139−7145.
24. Veal, J. M., and Brown, F. K. (1995) *J. Am. Chem. Soc. 117*, 1873−1880.
25. Gao, X., Rice, J. S., Cross, C. W., and Yang, X. (1997) *Nucleosides Nucleotides 16*, 1599−1608.
26. Heinemann, U., Rudolph, L.-N., Claudis, A., Morr, M., Heikens, R. F., and Blocker, H. (1991) *Nucleic Acids Res. 19*, 427−433.
27. Hausheer, F. H., Rao, B. G., Saxe, J. D., and Singh, U. C. (1992) *J. Am. Chem. Soc. 114*, 3201−3206.
28. Luo, P., Leitzel, J. C., Zhan, Z.-Y. J., and Lynn, D. G. (1998) *J. Am. Chem. Soc. 120*, 3019−3031.
29. Bachelin, B., Hessler, G., Kurz, G., Hacia, J. G., Dervan, P. B., and Kessler, H. (1998) *Nat. Struct. Biol. 5*, 271−276.
30. Gyi, J. I., Lane, A. N., Conn, G. L., and Brown, T. (1998) *Biochemistry 37*, 73−80.

BI990456X